Control No. AP253

EFFECT OF A DENSITY EXTREMUM ON

LOCK EXCHANGE FLOW

by

Yehia R. Marmoush[1], Paul F. Hamblin[1],

and Alan A. Smith[2]

[1]National Water Research Institute
Canada Centre for Inland Waters
Burlington, Ontario, Canada
[2]Prof. Dept. of Civil Engineering
McMaster University, Hamilton, Ontario, Canada
NWRI Contribution #86- 202

EXECUTIVE SUMMARY

This manuscript summarizes the doctoral research activities of Y. Marmoush, Department of Civil Engineering McMaster University and is intended for an audience of fluid mechanicians, physical limnologists, geophysicists and power engineers.

The research topic of determining how to characterize the spreading of large heated discharges in lakes and in winter was sparked by the concern of the Ontario Ministry of Environment on the possible damage to nearshore whitefish spawning grounds if the spawn is subjected to unnaturally heated water during a critical stage of their development. In 1980 Ontario Hydro undertook an extensive series of winter thermal plume mappings which served as an observational basis for the research study reported herein.

By means of a somewhat idealized model of the winter thermal plume spreading referred to as the loch exchange flow, for the first time to our knowledge, this phenomenon was investigated in the case where the temperature of maximium density (4°C) plays a crucial role. In a laboratory experiment in the NWRI cold chamber the dramatic influence of the 4°C water was first demonstrated, and quantitative relations between the horizontal spreading distance and the background environmental relations where determined.

Development of a highly accurate mathematical model run at McMaster University served to further quantify the behaviour of the spreading thermal plume in parameter ranges not easily obtainable in the laboratory.

Finally, following from the insight gained in the above two studies, a detailed analysis of the key physical processes involved in the spreading and subsequent sinking processes permit simple expressions to be derived which both unify the numerical and experimental results and provide a predictive cabability for environmental applications.

An application of these spreading relations to the data collected at the Ontario Hydro site predicts the initial spreading phase up to the point of detachment of the headed discharge extremely well and the second phase from the point of detachment to the sinking zone in a reasonable fashion. It is thought that the neglect of offshore winds in the second phase probably contributed to the underestimation of the areal extent of the plumes during winter 1980.

ABSTRACT

The existence of a density extremum in water at 4°C gives rise to densimetric flows, which are markedly different from those in the linear range. Experimental, numerical and scaling investigations are described that give some insight into the overflow and sinking processes in a lock exchange flow and the manner in which they may influence nearshore transport in the vicinity of a thermal outfall in a cold climate. The investigations were restricted to an idealized model where the lock exchange mechanism was selected due to the fact that its behaviour is close to that expected in the prototype situation. A simple application illustrates how the results obtained might be employed in the design of power station circulating water systems that must operate in severe winter conditions.

1. INTRODUCTION

In power station once-through cooling water systems, the waste heat is discharged to the environment in the form of heated effluent with a temperature typically 10C° above that of the receiving water. Under the temperate climatic conditions which commonly obtain, this warm water forms a raft with a pronounced discontinuity in the vertical temperature distribution. A front forms at the edge of the plume driven by the thermal density difference. When sufficiently large stations are located adjacent to natural bodies of water, their warm water discharges give rise to environmental concerns which are frequently more important than the technical problem of warm surface water being drawn into the cooling water intake with consequent reduction in the thermal and economic efficiency of the station. The transport of heat by buoyancy-induced convective motions is a mechanism which finds relevance in many physical systems. Accordingly, there have been numerous theoretical, experimental and numerical studies of various aspects of natural convective flows. Usually the direct modelling of these natural systems is very complex; however, certain idealized cases of such convective motions provide some insight into these more difficult problems. To analyse the principal flow regime in an idealized case which is likely to occur in the vicinity of a thermal outfall, the lock exchange mechanism is usually selected due to the fact that its behaviour is close to that expected in a prototype situation. The phenomenon of lock exchange flow is the classical case of unsteady non-uniform flow in the field of small density difference hydraulics. This phenomenon occurs when a lock gate or other such division separates bodies of still water with the same surface elevation but which differ slightly in density. While the opening of the gate may result in local disturbances, the predominant effect will be a continuing exchange pattern of flow which is caused by the density difference. Experimental studies of thermal densimetric flow have been reported by a large number of investigators. Keulegan (1946, 1957) and Schijf and Schonfeld (1953) used salinity as the density difference agency, whereas Barr (1963, 1966, 1967) and Didden and Maxworthy (1982) used both thermally and salinity induced density flows. Recently, Simpson (1982) has given a broad-ranging account of gravity currents (which includes a most comprehensive bibliography).

In cold climates, the behaviour of thermal density currents may be altered when the receiving water is close to the freezing point and when the discharge water has a temperature higher than the temperature of maximum density (4°C). Temperatures higher than the ambient have been observed near the bottom of fresh water lakes in the vicinity of thermal discharges [Pipes _et al_. (1973) and Metcalfe (1980)]. Concern has been expressed about the adverse effects of such abnormally warm water on the winter ecology of lakes in cold climates [Hoglund and Spigarelli (1972)]. It is expected that the existence of a density extremum in water at 4°C and the nonlinear relation between density and temperature cause densimetric flows which are markedly different from those in the linear range. When an ambient temperature of close to 0°C is assumed, thermal discharges warmer than 8°C will have positive buoyancy and spread as a surface layer. Thereafter, the plume will begin to sink when its temperature is brought to less than 8°C by cooling and mixing processes since at this point its density is greater than that of the receiving fluid. This sinking warm water will then spread over the bed as a density current subjecting life forms on the lake bed to a transient and unseasonal increase in temperature. The sinking phenomenon, termed the thermal bar in the geophysical literature, may occur in the vicinity of man-made warm effluents and also in natural bodies of water during the spring warming period as reported by Rodgers (1968) and Spain et al. (1976).

The fluid mechanics of the convecting flows with a density extremum are less well known than the lock exchange or gravity current phenomenon. The information given by the numerical study of Robillard and Vasseur (1982) and the laboratory investigations of Inaba and Fukuda (1984) concerning the effect of density inversion of water near 4°C on the natural convective motion in an enclosed cavity provide some insight into this problem, but not sufficient for understanding the heated discharge problem due to its highly transient nature. In the study to be described, lock exchange flows were produced between two bodies of water having asymmetrical temperatures around 4°C. The behaviour of these flows is expected to demonstrate the influence of a density extremum on lock exchange which is close to that found in a prototype situation. Laboratory and numerical analyses were carried out to confirm the existence of the sinking plume phenomenon and to allow more detailed study of the zones upstream and downstream of the 4° isotherm as well as the plunging region at the front.

2. PHYSICAL EXPERIMENTS

A series of physical experiments were conducted in a cold chamber to investigate the phenomenon of the sinking plume in lock exchange flows. The densimetric flows were created in a horizontal flume where a vertical barrier which was located asymmetrically along the length of the channel was carefully removed. The shorter portion was used to contain the warm water. Weirs were fitted at each end of the flume to provide the same depth on both sides of the barrier. Thermistors were arranged vertically along the centre line of the flume to be uniformly spaced over the depth of water used in the test. More details of experimental apparatus may be found in Marmoush et al. (1984).

Because of the effects of distant boundaries of the laboratory apparatus which are unlike those in a natural environment, interest was focussed on the initial occurrence of the plunging plume and the arresting of the overflow. The temperature of the cold reservoir, T_c, was set so that $0 \leq T_c < 4°C$ and similarly the warm reservoir temperature, T_w, was adjusted such that $T_w > 8°C$. The initial flow pattern was similar to the classical lock exchange mechanism; the warmer buoyant layer which was identified with a weak trace of fluorescene, extended over the cold receiving water. Concurrently, a cold, dense wedge was propagated under the warm body of water. The visual impression given by the dyed water was that the fluid behind the advancing front was turbulent. After the warm front had progressed for some distance, filaments of fluorescene dyed water could be seen extending downwards from the interface through the colder water to the bed of the flume. As the volume of water entrained in this way increased, the warm front was arrested and a layer of dyed water was seen to propagate along the bed of the flume in the same direction as the original surface layer. The three zones of interest in the vicinity of 4° isotherm were clearly demonstrated viz. (i) the thermal overflow region, (ii) the thermal front, and (iii) the thermal underflow region. The experiments provide dramatic proof that the existence of an extremum in the density-temperature relation has a profound influence on the behaviour of densimetric flows. Before presenting the effect of varying laboratory conditions on the initial behaviour of overflow and sinking processes we first discuss possible means of quantifying experimental results of this kind.

DISCUSSION OF EXPERIMENTAL RESULTS

One approach to quantify these effects is through the use of the Rayleigh number. The Rayleigh number is defined as

$$R_a = g(\Delta\rho)H^3/\rho_o \nu_o \kappa_o \tag{1}$$

where $\Delta\rho$ is the density difference between the two water bodies, H is the depth of water in the flume, g is the gravitational acceleration, and ρ_o, ν_o, κ_o are the fluid properties (density, kinematic viscosity and thermal conductivity, respectively) at a specified reference temperature of T_o=4°C. Due to laboratory limitations, fairly large experimental Rayleigh numbers were used with values ranging from 10^7 to 10^8.

The convective motions under investigation here are produced by a difference in density (i.e. due to a temperature gradient). Generally in convection problems, the flow patterns are dependent mainly on the specified values of the Rayleigh number R_a, Prandtl number P_r (ν/κ) and aspect ratio A (Length, L / Depth, H). Numerical simulation of convective motions for circumstances in which the density-temperature dependence is linear, can be categorized by a single Rayleigh number as defined in Eq. 1. However, when a nonlinear density-temperature relation is involved and specifically when the warm and cold temperatures are separated by the temperature of maximum density, it is necessary to employ three different definitions of Rayleigh numbers to completely describe the experiment. These three values are:

1-the cold Rayleigh number, $(R_a)_c = g(\rho_4 - \rho_c)H^3/\rho_o \nu_o \kappa_o$ (1.a)

2-the warm Rayleigh number, $(R_a)_w = g(\rho_4 - \rho_w)H^3/\rho_o \nu_o \kappa_o$ (1.b)

3-the lock exchange Rayleigh number, $(R_a)_l = g(\rho_c - \rho_w)H^3/\rho_o \nu_o \kappa_o)$ (1.c)

From these definitions, it is apparent that any one Rayleigh number is dependent on the other two. In the investigation described here, $(R_a)_c$ and $(R_a)_l$ are considered to be independent parameters with the dependent $(R_a)_w = (R_a)_c + (R_a)_l$*. If symmetrical temperature differences around 4°C are assumed, $(R_a)_c = (R_a)_w$, (so that $(R_a)_l = 0$) and only one of these is sufficient to describe the behaviour. The other determining parameter of the flow, the Prandtl number, is temperature dependent and has values of 11.6, 9.0 and 7.0 for specified temperatures of 4°C, 15°C and 20°C, respectively (due mainly to the change in kinematic viscosity). Unlike the case of the conventional cavity convection problem [Patterson and Imberger (1980), Hamblin and Ivey (1984)], in which R_a, P_r and A specify the flow pattern, the lock exchange flow mechanism is a function of $(R_a)_l$, $(R_a)_c$ and P_r.

---

* For the unlikely case that 4°C < T_w < 8°C the lock exchange $(R_a)_l$ will be negative by the above definition indicating that lock exchange will occur but in a reverse direction, i.e. cold buoyant water overlying the warmer water.

When the distance that the plume travels horizontally before it sinks to the bottom is non-dimensionalized with respect to the depth, it becomes effectively the aspect ratio of the convective flow pattern, a quantity to be determined and not specified. Hence, the objective is to find the dependence of the aspect ratio A on the independent parameters, $(R_a)_1$, $(R_a)_c$, and P_r. After the plume sinks there will be a slow lateral migration of the sinking point as the fluid tends towards its final rest state. However, this stage is of little interest and will not be considered further.

All the tests in the experimental investigation were carried out with the cold water temperature close to 0°C for ease of control. Thus the effect of the variation of $(R_a)_c$, caused by different cold water temperatures, was not examined. Since P_r is a function of temperature for any specific fluid it is therefore subject to minor spatial variations between warm and cold zones in the laboratory experiments. For calculation purposes, a constant value was assumed and defined at a reference temperature of 4°C. A number of observations of the horizontal extension distance were taken with varying warm water temperature and depths, as listed in Table 1.

The experimental parameters described in these tests are used to determine the relation between the maximum extension of the upper layer L_{max}/H and the system parameters $[(R_a)_1, (R_a)_c]$. These results will be displayed in a later section along with additional values obtained by the solution of a mathematical model. From the experimental data, it was found that L_{max}/H is proportional to $(R_a)_1^{+.5}$ and to $(R_a)_c^{-.5}$.

3. MATHEMATICAL FORMULATION OF THE PROBLEM

The fluid motion and heat transfer are generally described by a set (system) of coupled (simultaneous) partial differential equations which are mathematical statements of the conservation of momentum, energy and mass. Moreover, the equation of state for the fluid of interest must be defined over the temperature range to be simulated. The system of equations comprises: (i) the Navier-Stokes equation (conservation of momentum), (ii) the heat-transfer equation (conservation of energy), (iii) the continuity equation (conservation of mass), and (iv) the equation of state for the fluid (density-temperature relationship). Thus for a fluid element the two-dimensional governing differential equations [Lamb (1945) and Schlichting (1968)] are:

$$\frac{\partial u}{\partial t} + u\frac{\partial u}{\partial x} + v\frac{\partial u}{\partial y} = \frac{-1}{\rho_o}\frac{\partial p}{\partial x} + \nu_o\nabla^2 u \qquad (2)$$

$$\frac{\partial v}{\partial t} + u\frac{\partial v}{\partial x} + v\frac{\partial v}{\partial y} = \frac{-1}{\rho_o}\frac{\partial p}{\partial y} + \nu_o\nabla^2 v - g\frac{\Delta\rho}{\rho_o} \qquad (3)$$

$$\frac{\partial T}{\partial t} + u\frac{\partial T}{\partial x} + v\frac{\partial T}{\partial y} = \kappa_o\nabla^2 T \qquad (4)$$

$$\frac{\partial u}{\partial x} + \frac{\partial u}{\partial y} = 0 \qquad (5)$$

$$\rho = \rho_o[1 - \beta(T-T_o)^2] \qquad (6)$$

The equations are written in an Eulerian frame of reference where u and v are the horizontal and vertical components of the velocity field, T is the temperature of fluid, p is the pressure, t is the time, and x and y are the coordinates of elements in the horizontal and vertical directions (Fig. 1a). It is assumed that the fluid is incompressible and follows a Newtonian shear stress law. Moreover, the Boussinesq approximation is applied [Gray and Giorgini (1976)].

By defining the component of vorticity in the x-y plane as $\omega = \partial u/\partial y - \partial v/\partial x$, equations (2) and (3) yield the following vorticity-transport equation

$$\frac{\partial \omega}{\partial t} + u\frac{\partial \omega}{\partial x} + v\frac{\partial \omega}{\partial y} = \nu_o \nabla^2 \omega + g\frac{\partial}{\partial x}\left(\frac{\Delta\rho}{\rho_o}\right) \tag{7}$$

The stream-function ψ is described by the relations $\partial\psi/\partial y = -u$ and $\partial\psi/\partial x = v$, so that

$$\frac{\partial^2\psi}{\partial x^2} + \frac{\partial^2\psi}{\partial y^2} = -\omega \tag{8a}$$

or

$$\nabla^2\psi = -\omega \tag{8b}$$

It is noted that the continuity equation, (5), is identically satisfied by the introduction of the stream-function, ψ. The governing differential equation can be normalized by defining the following non-dimensional terms

$$X = x/H \quad ; \quad Y = y/H \quad ; \quad \tau = t\kappa_o/H^2 \; ; \; U = uH/\kappa_o \quad ;$$
$$V = vH/\kappa_o \; ; \; \Omega = \omega H^2/\kappa_o \; ; \; \Psi = \psi/\kappa_o \quad ; \; \theta = (T-T_o)/\Delta T \; , \qquad (9)$$

where the water depth, H, is the characteristic length and ΔT is the temperature difference between the two water bodies. Due to the semi-infinite nature of the domain of interest, it is not possible to normalize the equations in terms of any characteristic horizontal length. Substituting the terms of (9) into the governing differential equations, the normalized conservative system of equations becomes

$$\frac{\partial \theta}{\partial \tau} + \frac{\partial U\theta}{\partial X} + \frac{\partial V\theta}{\partial Y} = \nabla^2\theta \qquad (10)$$

$$\frac{\partial \Omega}{\partial \tau} + \frac{\partial U\Omega}{\partial X} + \frac{\partial V\Omega}{\partial Y} = P_r\nabla^2\Omega - (R_a)_o P_r \frac{\partial \theta^2}{\partial X} \qquad (11)$$

$$\nabla^2\Psi = -\Omega \qquad (12)$$

$$U = -\frac{\partial \Psi}{\partial Y} \quad , \quad V = \frac{\partial \Psi}{\partial X} \qquad (13)$$

where $(R_a)_o$ is equal to $g\beta(\Delta T)^2H^3/\nu_o\kappa_o$. The relation between $(R_a)_o$ and the other definitions of Rayleigh numbers can be found in Table 2. The investigation is carried out for the lock exchange flows shown in Figure 1(b). The associated non-dimensional initial and boundary conditions, shown in Figure 1(b), are detailed in (14) and (15).

For $\tau \leq 0$: $\quad U = V = \Psi = \Omega = 0 \quad$, everywhere $\qquad (14)$

$$\theta = \theta_w \quad , \text{ at } X<0$$
$$\theta = (\theta_c + \theta_w)/2 \quad , \text{ at } X=0$$
$$\theta = \theta_c \quad , \text{ at } X>0 \qquad (15)$$

For $\tau > 0$: $U = \partial V/\partial X = \Psi = \partial\theta/\partial X = \Omega = 0$, at $X=\pm\infty$

$\partial U/\partial Y = V = \Psi = \partial\theta/\partial Y = \Omega = 0$, at $Y=0,1$

A "no-slip" condition at the lower boundary is not specified due to the increase in the cost of numerical simulation which this would incur (see section 4). A slip boundary condition is judged to be acceptable since interest is concentrated on the penetration of the upper layer and not the details of the wall boundary layers.

4. NUMERICAL ANALYSIS

A numerical procedure has been developed to model the behaviour of a thermal front at the outfall of an electric generating station cooling water system [Marmoush (1985)]. The numerical model employs a finite-difference scheme where the resulting algebraic finite difference equations are solved using an alternating direction implicit (ADI) method and a sparse-matrix package. The numerical model has been verified by comparing it to numerical solutions of four different cases of the idealized problem of steady laminar flow in an enclosed rectangular cavity with differentially heated end walls. Moreover, additional acceleration techniques have been introduced to improve the numerical solution procedure [Marmoush _et al_. (1985)].

The general behaviour will be discussed for a numerical run where the values of the lock exchange $[(R_a)_l]$ and cold $[(R_a)_c]$ Rayleigh numbers are assumed to be 15000 and 1000, respectively. These two chosen values of Rayleigh numbers correspond to warm (θ_w) and cold (θ_c) dimensionless temperatures of +0.8 and -0.2, respectively. The Prandtl number P_r is assumed to have a value of 11.6 which is the value corresponding to a reference temperature of 4°C. This run is designated as Run #6 in Table 2. As the extent of the frontal disturbance increased following the (simulated) removal of the barrier, the computational domain was extended in a series of steps so as to always contain the region of interest. In general the computational domain is larger than that depicted in Figures 2 and 3. The following observations may be made from the computational results obtained.

1) The initial behaviour is governed by the difference in horizontal pressure and closely resembles the classical lock exchange mechanism. The warm water extends as an upper layer, while the cold water extends in the opposite direction as a lower layer. As the motion of both layers is governed by the lock exchange process, almost symmetrical behaviour of both layers around the barrier is to be expected.

2) As the relative extension distance between the upper and lower fronts increases, the heat transfer between the two layers causes a reduction in the buoyancy driving force.

The asymmetrical behaviour shown in Figure 2 is explained by the nonlinear response of density to change of temperature in the warm and cold layers.

3) Due to the continuous reduction of the horizontal inertia and mixing at the warm front, the diluted water near the front attains the temperature of maximum density ($\theta = 0$, $T = 4°C$). This maximum density water then sinks vertically from the upper layer and is entrained by the lower layer which results in an increase of the temperature of the lower layer. The location of this sinking phenomenon can be identified as the point at which the isotherm for $\theta = 0$ ($T = 4°C$) is vertical through the upper layer. Eventually this 0°C isotherm will extend throughout the total depth of the lock exchange flow.

4) Due to the phenomenon described in (3) above, the sinking frontal extremity of the upper layer forms a closed convective cell. Forward movement of the upper front ceases at this stage.

5) The temperature gradient created between the cold water and the thermal front drives a compensating convective cell in the cold region as shown in Figure 3.

6) Thereafter, the simulated domain is divided into two convective cells of opposite rotational sense on either side of the location of the thermal front. Each of these is governed by the gradient between the "ambient" water

temperature (θ_w or θ_c) and the temperature of maximum density ($\theta = 0$). Both cells transport "ambient" water towards and away from the thermal front location through the upper and lower layers respectively.

To reduce the computational cost, the numerical calculation was stopped when the thermal front location showed an acceptably small variation with the elapsed time. It should be noted, however, that this point is not a final equilibrium state but it is considered to represent the point at which the horizontal extension is arrested by the vertical sinking. The maximum extension of the thermal front is taken at the distance L/H at which the upper penetration of the 4°C isotherm reaches a quasi-steady state.

For a densimetric flow between two water bodies having different temperatures around 4°C, the flow pattern can be described in terms of three zones of interest. These three zones which are shown schematically in Figure 4, Figure 4(a) and 4(b) are expressed in terms of dimensional and non-dimensional parameters, respectively. Over one of these zones, the densimetric flow is maintained by the density differences between the thermal front (i.e. $\theta = 0$, or $T = 4$°C) and the warm water body (i.e. $\theta = \theta_w$, or $T = T_w$). Two warm layers having different temperatures, both more than 4°C ($\theta > 0$) and less than T_w ($\theta < \theta_w$) are established. The convective motion in this zone will be identified as a warm convective cell which transports the ambient warm water to the thermal front, where the water approaches maximum density, sinks and by continuity returns as a reversed underflow. In the other zone, the densimetric flow is maintained by the density differences between the thermal front (i.e. $\theta = 0$, or $T = 4°C$) and the cold water body (i.e. $\theta = \theta_c$, or $T = T_c$). Two cold layers having different temperatures, both less than 4°C ($\theta < 0$) and more than T_c ($\theta > \theta_c$) are established. The convective motion in this zone will be identified as a cold convective cell which transports the ambient cold water to the thermal front, and behaves in a similar manner to the warm front. It should be noted that for both warm and cold convective cells, the layers are vertically stable. Between these two zones (i.e. the warm and cold convective cells), the thermal front exists forming the third zone and showing a constant vertical temperature $\theta = 0$ (i.e. $T = 4°C$).

The aspect ratio, A, will be determined by $(R_a)_1$, $(R_a)_c$, and P_r as long as the numerical domains are essentially semi-infinite and free from boundary reflection effects such as those described by Simpson (1982).

The sensitivity of L_{max}/H or A to the variation of each parameter was examined numerically. The calculated values of L_{max}/H and model parameters are listed in Table 2. By examining the sensitivity of L_{max}/H with respect to each of the parameters separately, it is found that L_{max}/H is proportional to $(R_a)_1^{+0.50}$ and $(R_a)_c^{-0.36}$. For small values of $(R_a)_1$, L_{max}/H is not sensitive to P_r, but for high values of $(R_a)_1$, it is proportional to $[P_r]^{-0.15}$.

It is worth mentioning that due to the limitation on the maximum size of $(R_a)_1$ which could be simulated with the available computational resources, the correlation with respect to P_r is far from conclusive. A comparison of the numerical with the experimental results will be deferred until the next section in which scaling analysis is discussed.

5. EXTENSION DISTANCE RELATIONS

The estimated value of the maximum extension distance of the thermal front (L_{max}) can be related to the relevant parameters by using a scaling analysis approach. The laboratory experiment suggests that for higher values of $(R_a)_1$, the penetration of the upper layer is governed by inertial forces. Therefore, the scale of the horizontal velocity of the upper layer, u, may be estimated from the balance between horizontal advection and the opposing horizontal pressure forces in the horizontal momentum equation (2), which yields

$$\frac{u^2}{L} \sim \frac{\Delta p}{\rho_o L} \sim \frac{g \Delta\rho_1}{\rho_o L} H$$

$$\text{or} \quad u = C_1 \sqrt{g \frac{\Delta\rho_1}{\rho_o} H} \qquad (16)$$

Similarly, from the vertical balance of inertia and buoyancy the scale of the vertical sinking velocity of the upper layer, v, may be estimated from the balance between either horizontal or vertical advection and the vertical buoyancy forces in the vertical momentum equation (3). This balance yields $vu/L \sim g\ \Delta\rho c/\rho o$, i.e.

$$v \sim g \frac{\Delta\rho_c}{\rho_o} \frac{L_{max}}{u} \qquad (1$$

The maximum horizontal extension distance, L_{max}, of the thermal front is achieved when the continuity equation (5) is satisfied, i.e. $u/L_{max} \sim v/H$, and combining with Eqns. (16) and (17) we obtain,

$$\frac{L_{max}}{H} = C_2 (R_a)_1^{1/2} (R_a)_c^{-1/2} \qquad (18$$

For smaller values of $(R_a)_1$, the numerical experiments suggest that viscous forces may not be neglected in the sinking process. In this case, the vertical sinking velocity may be estimated from the theory of convection between horizontal plates. Where the buoyancy flux depends on the conditions very near the boundaries and is independent of the plate separation and of P_r, the following relation is found (Turner, 1973)

$$Nu \sim (R_a)_c^{1/3} \qquad (19$$

where Nu is the Nusselt number which is defined as $Nu \sim v\Delta TH/\kappa\Delta T$. Consequently, Eqn. 17 will yield

$$v \sim \frac{\kappa}{H} (R_a)_c^{1/3} \qquad (20$$

Following the same arguments for the horizontal velocity scale, and the continuity equation, the following relation may be obtained

$$\frac{L_{max}}{H} = C_3 P_r^{1/2} (R_a)_1^{1/2} (R_a)_c^{-1/3} \quad (21)$$

It is of interest to note that for low values of P_r, Kraichnan (1962) predicted Nu as

$$Nu \sim P_r^{1/3} (R_a)_c^{1/3} \quad (22)$$

In this case, Eqn. 21 becomes

$$\frac{L_{max}}{H} = C_4 P_r^{1/6} (R_a)_1^{1/2} (R_a)_c^{-1/3} \quad (23)$$

A criterion for establishing which of the above relations apply may be estimated by considering the time taken for the development of a viscous boundary layer and by comparing this time to that required for a particle to travel a distance L in the horizontal or H in the vertical. If say $H^2/\nu < H/v$ viscous forces predominate or if from (16) and (21)

$$(R_a)_c^{1/3} < \frac{C_3}{C_1} P_r \quad \text{then}$$

relation (21) ought to apply. Alternatively, if $H^2/\nu > H/v$ or from (16) and (18), $(R_a)_c > (C_2/C_1)^2 P_r$ then the spreading process should be given by (18).

DISCUSSION

The relations derived in the preceding section for the horizontal spreading of the overflow contain an undetermined factor of proportionality. On account of the complexity of the flow, these factors are determined experimentally once the order of magnitude dependence of the independent parameters have been verified. In Figure 5 the laboratory results and the numerical results confirm the predicted exponents in equation (18) and (23) for each regime with the exception of the Prandtl number dependence in equation (23). The result of the numerical experiment no. 12 shown in Figure 5 would suggest a small negative exponent (~-.1) for the Prandtl number as opposed to the one-half power predicted by the scaling analysis. For this reason, the Prandtl number was not included in the variables plotted in Figure 5.

From the laboratory results of Barr (1963), C_1 was determined to be 0.55 which may be compared with that inferred from the initial spreading in the numerical experiments of 0.34. From our laboratory experiment C_2 in equation (18) is 11.(25) and C_3 is 0.2 from the numerical results. Based on these values we may establish the criteria for the regime boundaries more precisely. From the previous section the spreading process should be dominated by viscosity if $(R_a)_c < .05\ P_r^3$. In the light of the numerical results showing at most weak dependence on the Prandtl number, it is possible that this criterion should be $(R_a)_c < .05\ P_r^{3/2}$. In any case none of the experimental results were clearly dominated by viscous effects according to this criterion but were either in a transition between the two regime boundaries or in the case of the laboratory experiments were well above the inertially dominated boundary of $(R_a)_c > 418$ P_r. According to this criterion numerical experiment 12 should be marginally within the inertially dominated regime. This may explain why this point is shifted in Figure 5 towards the position of the laboratory-derived points.

APPLICATION

As an illustrative example of how some of the concepts developed in this study may be applied in a practical situation, we consider a set of eight field experiments in a winter outfall study conducted by Ontario Hydro (Metcalfe, 1980) in Lake Ontario. In the first stage of discharge, the heated plume spread out over the uniformly sloping bottom. The distance at which the buoyant plume detaches from the bottom may be estimated from the formula for axisymmetric spreading of a buoyant plume given by Didden and Maxworthy (1982). A preliminary analysis indicated that for typical values of the winter plume discharge, Q, of 100 m^3/s, eddy diffusivity of $3x10^{-3}$ m^2/s (Elliot, 1980) and reduced gravity, g^1 of 10^{-2} m/s^2, the initial stage would be governed by an inertia-buoyancy balance. With the assumption that the proportionality factors found by Didden and Maxworthy (1982) for the viscous-buoyancy range apply also in the inertia-buoyancy range, the radius, R, at which the discharge detaches from the sloping bottom is obtained as $R_1 = (1.2\ (4Q)\ /\ \sqrt{g^1 S^3})^{2/5}$ where S is the bottom slope. The multiplication of the discharge by a factor of 4 is an attempt to crudely account for the confining influence of the strong longshore currents present on all occasions. In the above expression, it is assumed that the discharge is contained within a single quadrant. This relation yields a distance R_1 of 700 m which is close to the observed distance of 500 m.

At this point, the further spreading of the plume is controlled by interplay of horizontal pressure forces and vertical sinking forces of the type of interest in this study. Since this application involves a continuous discharge and not a lock exchange flow, the axisymmetric inertial spreading formula of Didden and Maxworthy (1982) may be applied, i.e.

$$R_2 = .6\ (g^1\ 4Q)^{1/4}\ t^{3/4}\quad .$$

The time t may be estimated as $t = H/v$ where the vertical sinking velocity, v, is assumed to be given by our scaling analysis and experimental results for the inertially dominated range; thus

$$v = \frac{C_2}{C_1}\left(\frac{\kappa\nu}{H}(R_a)_c\right)^{1/2}.$$

Based on an observed depth of 8 m at the sinking point and an offshore water temperature of 2°C, the vertical sinking velocity is $2.3\ 10^{-3}$ m/s which results in the distance between the point of detachment and the sinking point of 390 m. This estimate may be compared to the average spreading distance beyond the point of detachment of about 1000 m observed over the eight experiments. The agreement between theory and observation is considered to be reasonable since during most field experiments offshore surface winds probably were responsible for spreading the plumes further offshore than under windless conditions.

It may be noted that other combinations of Didden and Maxworthy's spreading relations and the sinking relations, equations (18) and (21) may be applied in this manner to suit the circumstances of the environmental flow.

CONCLUSIONS

Stimulated by the need for an improved understanding of the dynamics of thermal discharges in winter in lakes, a series of laboratory and numerical experiments were carried out on the classical lock exchange mechanism in the presence of a density extremum. Attention focussed on the initial behaviour of the exchange flow and, in particular, on the dynamics of the arrested overflow and subsequent sinking of the plume at the temperature of maximum density. Comparison of the results with the classical lock exchange mechanism in a fluid with a linear temperature-density relation showed the profound influence of the nonlinearity in density on the flow field.

A number of parameters characterizing such flows are proposed, namely two distinct Rayleigh numbers and the Prandtl number as well as dependencies of the aspect ratio of the two-dimensional flow field on these numbers based on an elementary scaling analysis. These relations are generally supported by the laboratory and numerical experiments within narrow parameter ranges.

The analysis suggests other experiments of interest such as the case of the viscously dominated lock exchange flow. A more detailed exploration of the sinking process in the transitional range between viscous and inertial dominated convection and the further elaboration of the dependence of the aspect ratio on Prandtl number. Finally, we have demonstrated how our findings when combined with the relations on gravitational spreading established by Didden and Maxworthy (1982) may be employed to estimate the areal extent of a heated discharge in a cold receiving water body.

TABLE 1. Experimental Parameters

Test No.	H m	T_w, in C	T_c, in C	$(R_a)_w$ $*10^{-7}$	$(R_a)_c$ $*10^{-7}$	$(R_a)_1$ $*10^{-7}$	$(\frac{L_{max}}{H})$
1	0.10	18.20	0.00	6.761	0.538	6.223	42.5
2	0.10	14.15	0.00	3.453	0.538	2.915	30.0
3	0.10	12.15	0.30	2.230	0.459	1.771	23.5
4	0.10	12.14	0.05	2.221	0.524	1.697	22.5
5	0.15	10.80	0.25	5.243	1.588	3.655	16.7
6	0.15	18.15	0.45	22.646	1.433	21.213	43.3
7	0.15	12.45	0.70	8.082	1.234	6.847	23.2

Note: P_r = Constant = 11.6.

TABLE 2. Sensitivity of L_{max}/H to the variation of each parameter.

Run No.	Numerical Model Input Parameters θ_w	θ_c	P_r	$(R_a)_o$	Corresponding Physical Parameters $(R_a)_w$	$(R_a)_c$	$(R_a)_1$	$\frac{L_{max}}{H}$
1	+0.6	-0.4	11.6	625.0	225.0	100.0	125.0	1.0
2	+0.7	-0.3	11.6	1111.1	544.4	100.0	444.4	2.1
3	+0.8	-0.2	11.6	2500.0	1600.0	100.0	1500.0	3.5
4	+0.6	-0.4	11.6	6250.0	2250.0	1000.0	1250.0	1.8
5	+0.7	-0.3	11.6	11111.1	5444.4	1000.0	4444.4	3.3
6	+0.8	-0.2	11.6	25000.0	16000.0	1000.0	15000.0	6.2
7	+0.7	-0.3	11.6	3125.0	1531.3	281.3	1250.0	2.8
8	+0.8	-0.2	11.6	2083.3	1333.3	83.3	1250.0	4.5
9	+0.6	-0.4	11.6	75000.0	27000.0	12000.0	15000.0	2.5
10	+0.7	-0.3	11.6	37500.0	18375.0	3375.0	15000.0	4.0
11	+0.6	-0.4	5.0	6250.0	2250.0	1000.0	1250.0	1.8
12	+0.8	-0.2	1.0	25000.0	16000.0	1000.0	15000.0	8.9

$(R_a)_w = (R_a)_o\ [\theta_w^2]$
$(R_a)_c = (R_a)_o\ [\theta_c^2]$
$(R_a)_1 = (R_a)_o\ [\theta_w^2 - \theta_c^2]$

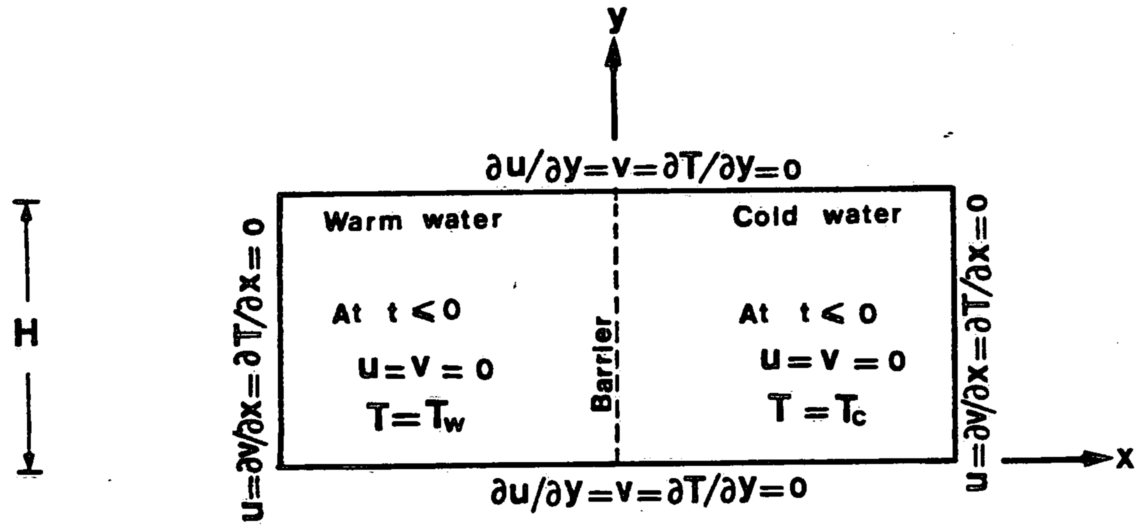
y
∂u/∂y=v=∂T/∂y=0
Warm water
Cold water
At t ≤ 0
u = v = 0
T=Tw
Barrier
At t ≤ 0
u = v = 0
T = Tc
H
u=∂v/∂x=∂T/∂x=0
u=∂v/∂x=∂T/∂x=0
x
∂u/∂y=v=∂T/∂y=0

(a)

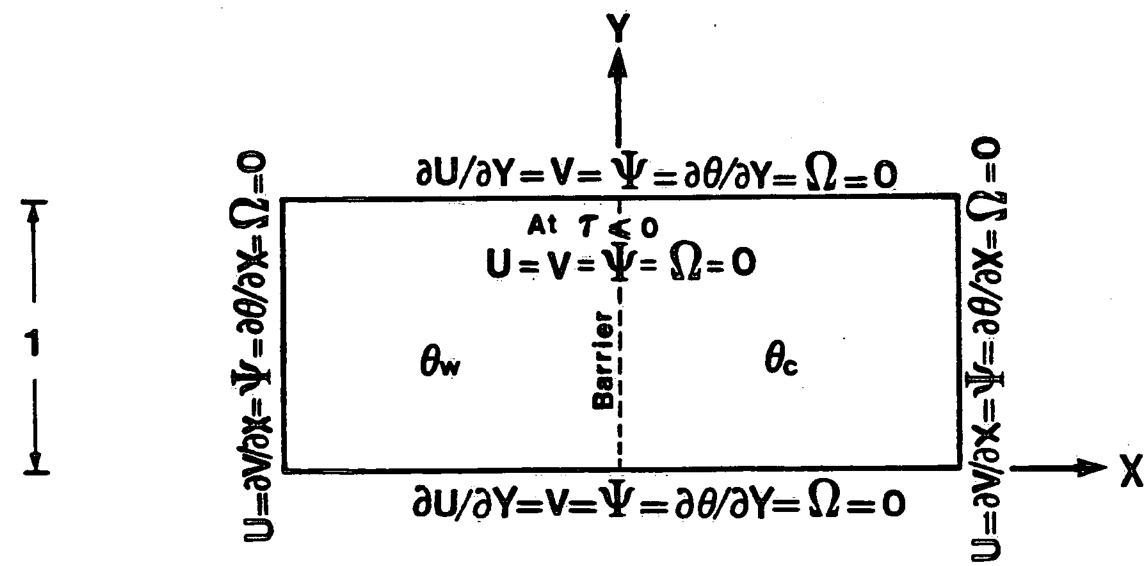
Y
∂U/∂Y=V=Ψ=∂θ/∂Y=Ω=0
At τ ≤ 0
U=V=Ψ=Ω=0
1
θw
Barrier
θc
U=∂V/∂X=Ψ=∂θ/∂X=Ω=0
U=∂V/∂X=Ψ=∂θ/∂X=Ω=0
X
∂U/∂Y=V=Ψ=∂θ/∂Y=Ω=0

(b)

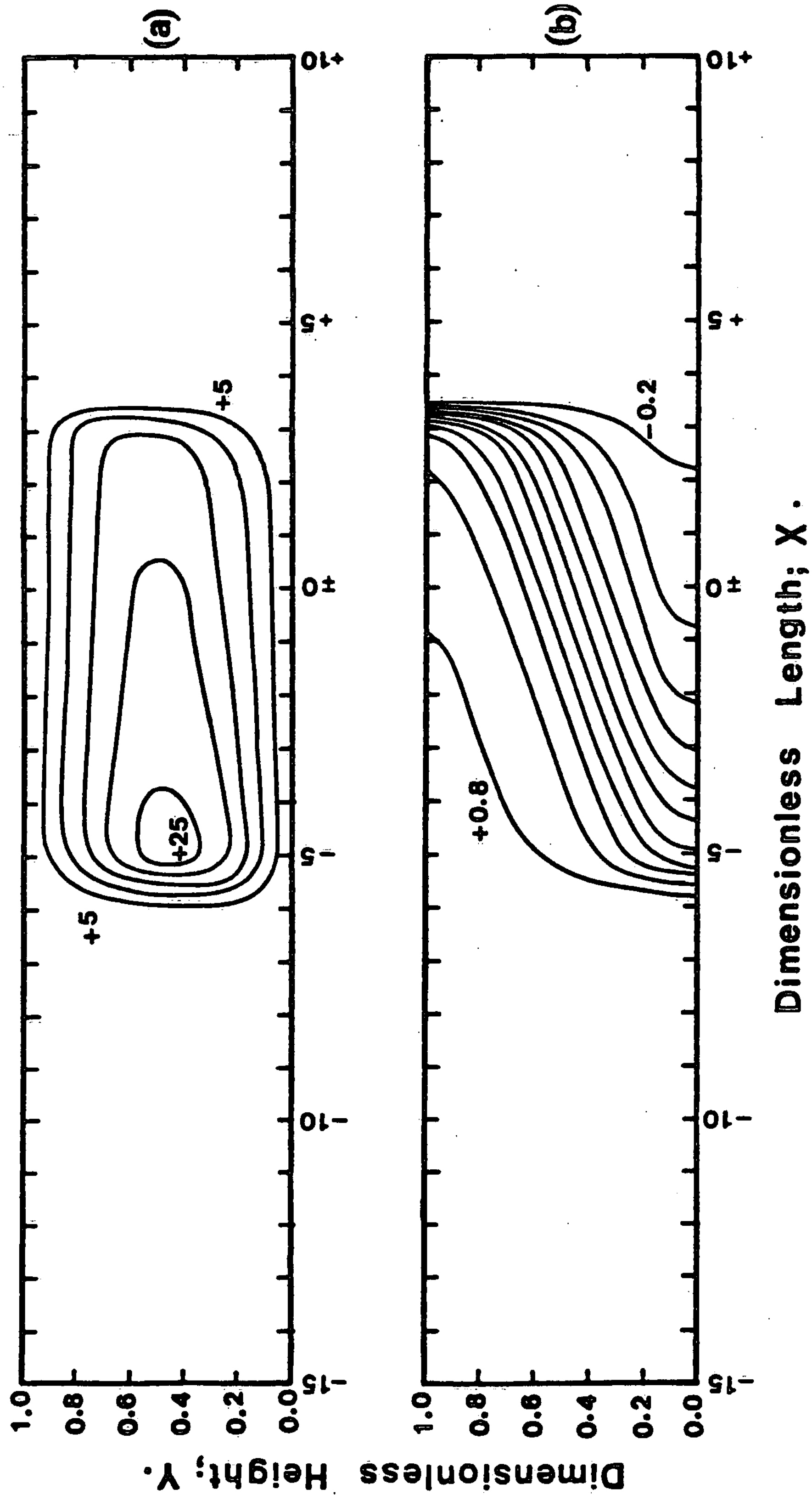
(a)
(b)
+5
+25
+5
−0.2
+0.8
Dimensionless Length; X.
Dimensionless Height; Y.
1.0
0.8
0.6
0.4
0.2
0.0
−15
−10
−5
±0
+5
+10

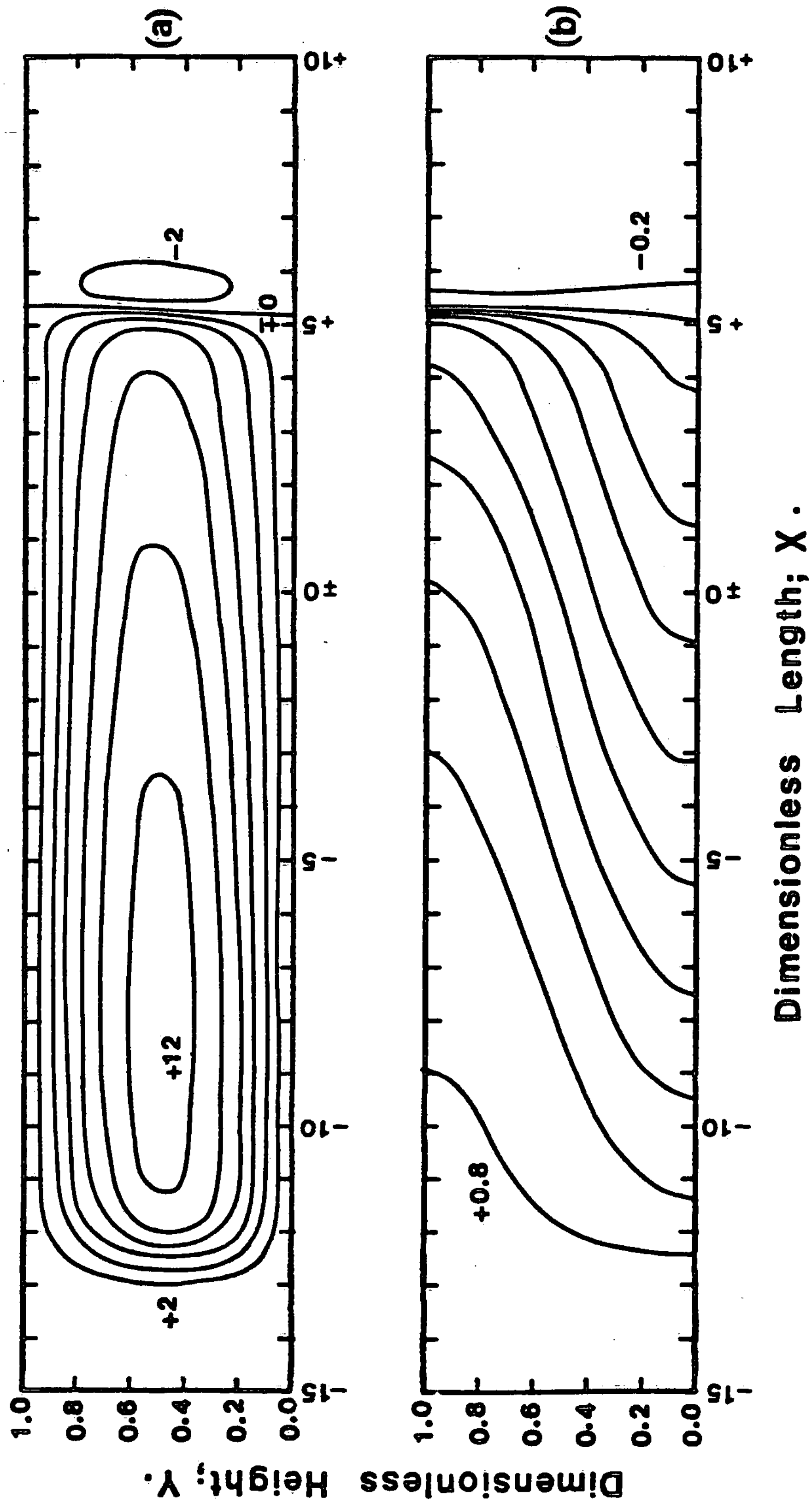
(a)
(b)
-2
±0
+12
+2
-0.2
+0.8
+10
+5
±0
-5
-10
-15
1.0
0.8
0.6
0.4
0.2
0.0
Dimensionless Length; X.
Dimensionless Height; Y.

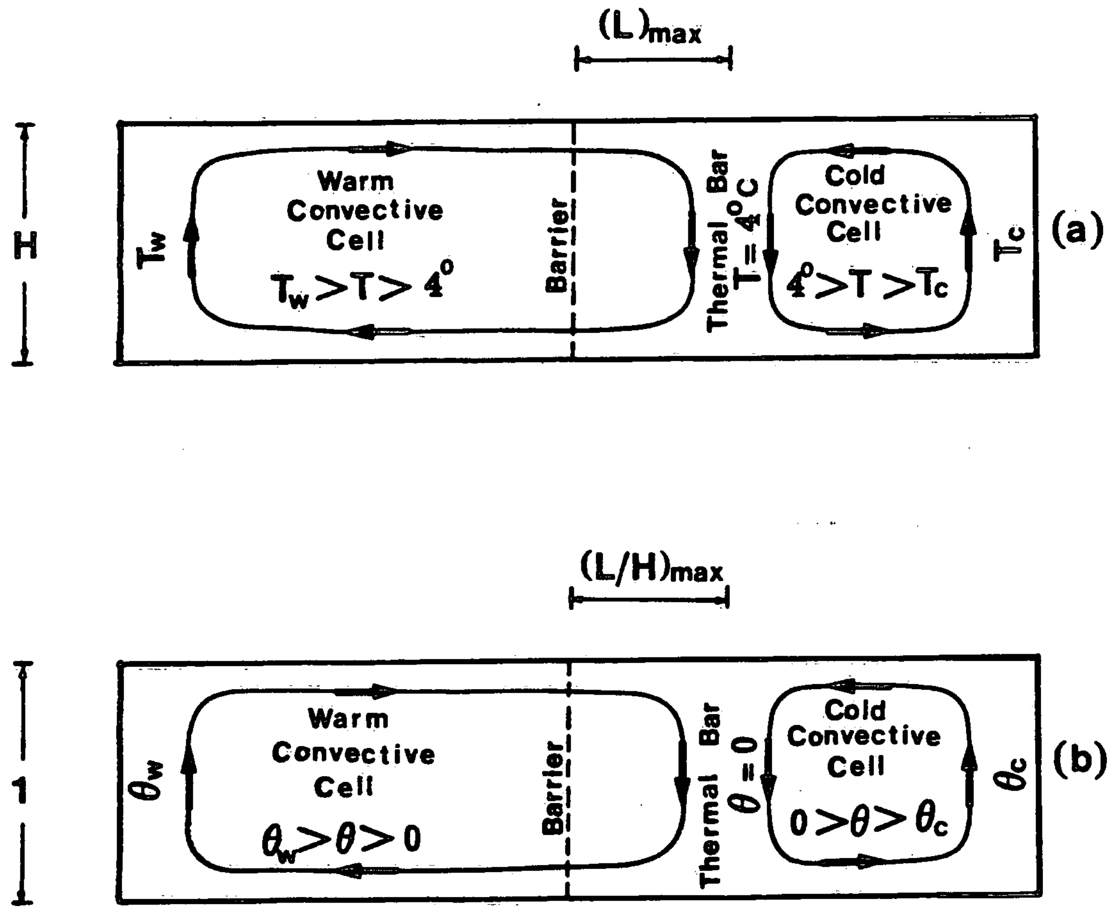
(L)max
H
Tw
Warm
Convective
Cell
Tw>T>4°
Barrier
Thermal Bar
T=4°C
Cold
Convective
Cell
4°>T>Tc
Tc
(a)
(L/H)max
1
θw
Warm
Convective
Cell
θw>θ>0
Barrier
Thermal Bar
θ=0
Cold
Convective
Cell
0>θ>θc
θc
(b)

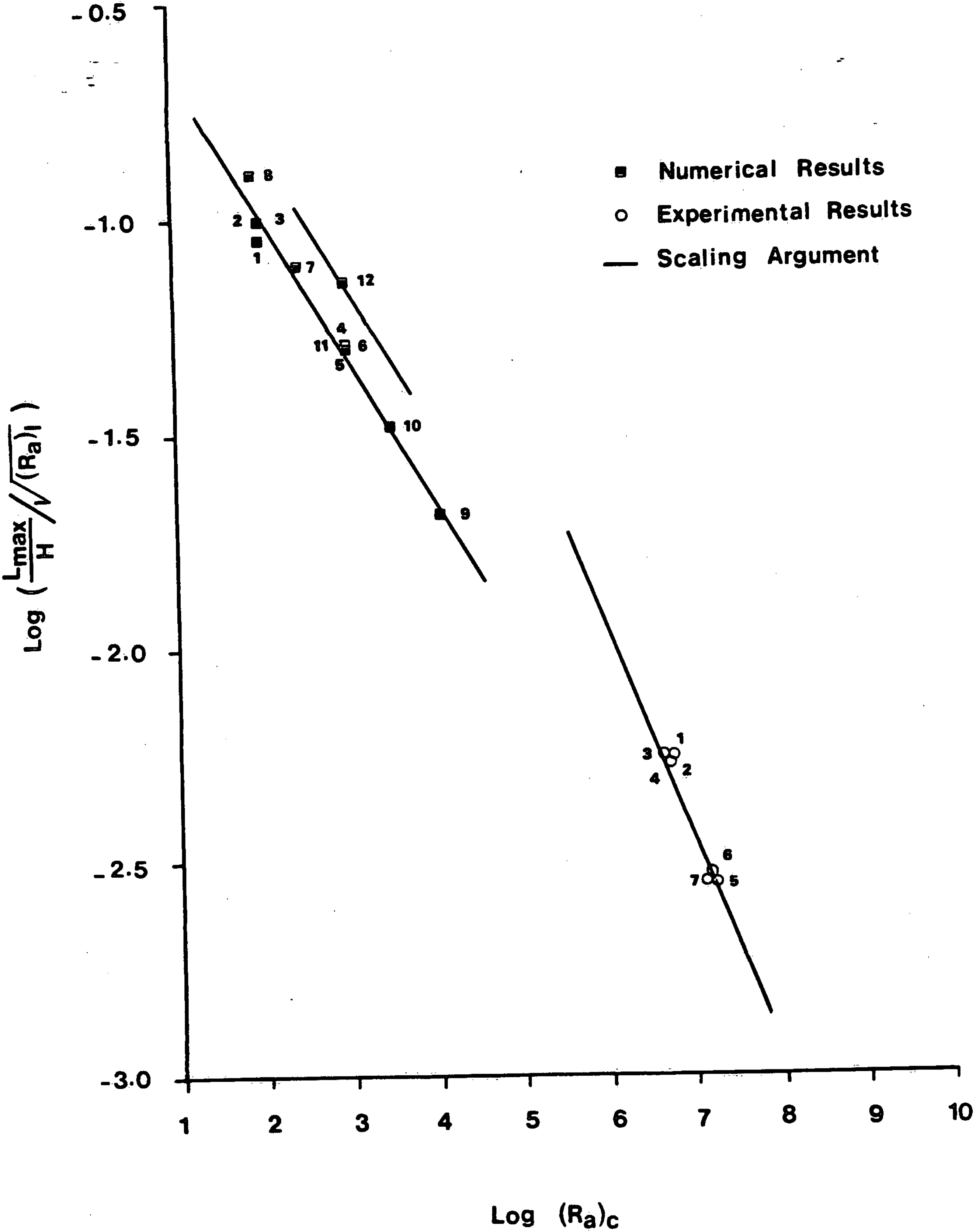
Numerical Results
Experimental Results
Scaling Argument
-0.5
-1.0
-1.5
-2.0
-2.5
-3.0
1
2
3
4
5
6
7
8
9
10
Log $(\frac{L_{max}}{H}/\sqrt{(R_a)_I})$
Log $(R_a)_c$